



# Seismic Resilience Assessment of the Hybrid Bridge Pier Based on Fragility Analysis

Jianpeng Sun<sup>1,2</sup> · Weichao Xu<sup>1,2</sup> · Zihan Tan<sup>1,2</sup>

Received: 8 June 2023 / Accepted: 18 February 2024 / Published online: 12 March 2024  
© Korean Society of Steel Construction 2024

## Abstract

At present, the seismic structure of recoverable functional bridges based on seismic resilience is one of the hotspots in bridge seismic engineering research. Therefore, a new type of hybrid piers is designed in this paper, which mainly relies on replaceable components to achieve repairable structural performance after earthquakes. At the same time, four-level seismic fortification objectives based on seismic resilience is proposed, and the follow-up stiffness phenomenon is found on this basis. The finite element software OPENSEES was used to perform IDA analysis on a hybrid pier and an ordinary reinforced concrete (RC) pier. The fragility curves and seismic resilience curves of two piers were compared, and the seismic resilience performance and the follow-up stiffness phenomenon of the hybrid pier were studied. The results show that under the action of different seismic waves, the top displacement angle of the pier of the hybrid pier is slightly larger than that of the ordinary RC pier, but the overall difference is not large. The fragility curve of the hybrid pier is slightly larger than that of the ordinary RC pier. However, with the damage to the hybrid pier, the follow-up stiffness phenomenon impacts the seismic performance, which reduces the seismic force acting on the structure and improves the seismic resilience of the structure. The post-earthquake recovery time of two piers under different damage states was determined. Combined with the fragility curves, the seismic resilience curves of two piers were presented. The resilient index of the hybrid pier was always maintained at 0.9–1, and the seismic resilience performance was excellent.

**Keywords** Hybrid bridge pier · Earthquake resilient structure · Follow-up stiffness · Fragility analysis · Seismic resilience

## 1 Introduction

The traditional seismic design concept aims at protecting life. Through ductile design, the brittle failure or even collapse of the structure under earthquake action is avoided, which provides the possibility of escape, and reduces the harm caused by the earthquake to a certain extent (ASCE, 2010; EN, 2005). However, during the action of the

earthquake, the main components such as piers are seriously damaged, and there is no clear index for the performance of the structure after earthquakes, resulting in the loss of its use function of the bridge structure, ignoring the consequences of the structure being unable to bear the original service load for a long time after earthquakes (Otsuka et al., 1999a, 1999b). Based on the understanding of bridge earthquake damage, scholars began to think about and study new bridge seismic structures with resilient characteristics such as recoverable, easy to repair, and avoiding brittle failure, so that the bridge can quickly restore its use function after earthquakes.

As an important force-bearing component of the bridge, the pier is one of the most common parts for researchers to arrange earthquake resilient structures. Guo et al. (2016) increased the energy dissipation mechanism based on the traditional swing self-centering pier to improve the seismic performance of the pier. Ou et al. (2006) improved the energy dissipation capacity of externally prestressed precast segmental columns by installing energy-dissipating

✉ Zihan Tan  
tanzihanyx@163.com

Jianpeng Sun  
sunjianpeng2001@163.com

Weichao Xu  
2287270229@qq.com

<sup>1</sup> School of Civil Engineering, Xi'an University of Architecture and Technology, Xi'an 710055, China

<sup>2</sup> Institute for Interdisciplinary and Innovate Research, Xi'an University of Architecture and Technology, Xi'an 710055, China

steel bars or yielding energy-dissipating devices at the joints of column segments. Rouse (2004) used fiber cement composite materials or steel sleeves to partially constrain concrete in the plastic hinge zone of prefabricated assembled columns with external prestressed segments. El-Bahey and Bruneau (2011, 2012) proposed to set the energy-consuming replaceable component between piers, and connect the energy-consuming replaceable component with the concrete-filled steel tubular pier column by using the joint plate to facilitate replacement. Dion et al. (2011) installed the energy dissipation damper between the abutment and the bridge deck and dissipated the earthquake energy through the damper, which effectively reduced the relative displacement between the abutment and the bridge deck and avoided the occurrence of falling beams. In addition, some scholars have studied the seismic performance of piers with additional replaceable components through experiments (Wang et al., 2018; Wang et al., 2022a, 2022b; Xia et al., 2021). The above studies show that these piers with earthquake resilient structures have good seismic performance and superior repairability.

At present, the realization of the seismic resilience of bridges has been recognized by the international earthquake engineering community and has become a research hotspot. Based on the theory of seismic resilience formed by Bruneau et al. (2003), Chang and Shinozuka (2004) and Manyena (2006), scholars have introduced the concept of seismic resilience into the study of bridge systems, but the research methods are different. Kiremidjian et al. (2007) used the San Francisco Bay Area as a test base to estimate the impact of site effects on bridge damage, including the assessment of bridge maintenance costs and the assessment of traffic network performance losses represented by travel time delays. Dong and Frangopol (2015) proposed a framework for probabilistic assessment of the seismic performance of highway bridges under main shock-after shock (MSAS). The probability of direct loss, indirect loss, and resilience of bridges under earthquake are studied. On this basis, a probabilistic framework for bridge seismic risk and resilience assessment based on the MSAS sequence is proposed. Frangopol and Bocchini (2011) proposed an evaluation index for the seismic resilience of bridges, which is related to the traffic capacity of bridges. Gidaris et al. (2017) studied the functional recovery model of highway bridges and then analyzed the seismic resilience of bridges under MSAS. Karamlou and Bocchini (2017) proposed the fragility-function surface based on the concept of bridge seismic fragility surface. Kilanitis and Sextos (2019a, 2019b) estimated the overall loss of earthquake damage to highway bridges and overpasses through more extensive network analysis rather than a single structural assessment. In addition, scholars have studied the seismic resilience of networks from different perspectives (Barker et al., 2013; Kilanitis

& Sextos, 2019a, 2019b; Ouyang et al., 2012; Paredes & Dueñas-Osorio, 2015; Reed et al., 2009; Sun et al., 2023).

Previous studies mainly focused on the optimal recovery sequence of bridges in the traffic network and the optimization design of a single bridge based on seismic resilience. There are few studies on the resilience evaluation and optimization design of bridge structural members. Scholars' research on the seismic performance of the structure under the original seismic fortification objective cannot evaluate the superiority of earthquake resilience structures. Therefore, it is necessary to propose a resilience evaluation method for bridge structural members that reflects repairability. The nonlinearity of the system is caused by the stress–strain nonlinearity of the material, which is called material nonlinearity. When the displacement of the structure makes the force of the system change significantly the analysis method of a linear system can not be used, which is called geometric nonlinearity. Previous studies have focused on material nonlinearity, such as using shape memory alloy (SMA) bars to replace ordinary steel bars in the plastic hinge zone of reinforced concrete columns or applying SMA bolts to self-centering steel column bases (Billah & Todorov, 2021; Zhu & Wang, 2021). Based on geometric nonlinearity, the author independently designed a hybrid pier and carried out calculations and analysis. The concept of follow-up stiffness is proposed, which shows that the structure has good geometric nonlinearity and can also improve the seismic resilience of the structure (Sun & Tan, 2022).

In this paper, a new type of hybrid piers is designed based on the research of damage distribution of reinforced concrete columns after earthquakes and the four-level seismic fortifications concept proposed by the fifth generation of the *Seismic Ground Motion Parameters Zonation Map of China* (GB, 2015; Li et al., 2021). On this basis, the concept of the follow-up stiffness is proposed, and the damage index of the pier is determined based on the displacement failure criterion. The seismic resilience evaluation of the hybrid pier considering post-earthquake repair time is carried out by using the proposed four-level seismic resilience fortifications concept and fragility curve. It can be seen from the fragility curves and the seismic resilience curves that the designed hybrid pier not only has good repairable performance but also has good seismic performance due to the follow-up stiffness phenomenon, which provides a reference for this kind of pier based on seismic resilience design in the future.

## 2 Fragility Analysis Method

Seismic fragility analysis is an effective evaluation method for the rationality of bridge damping systems (Elnashai & Sarno, 2015). It can evaluate the damage degree of the bridge under earthquake action, and establish an organic relationship

between the input intensity of ground motion and the damage index of the structure. It can grasp the possibility of structural damage under various potential earthquakes from a macro perspective, and then provide a theoretical basis for the evaluation of structural seismic resilience.

The probabilistic seismic demand model (PSDM) is the first step for seismic fragility analysis. The incremental dynamic analysis (IDA) method is commonly used. By adjusting the ground motion intensity (IM) of the seismic wave, the IDA method obtains the seismic response of the structural members under different ground motion intensities through a large number of dynamic time-history analyses, to establish a probabilistic seismic demand model.

The seismic fragility function can be expressed as

$$P(LS|PGA) = 1 - \Phi \left( \frac{\lambda_C - \lambda_{D|PGA}}{\sqrt{\beta_C^2 + \beta_{D|PGA}^2 + \beta_M^2}} \right) = \Phi \left( \frac{\ln m_{D|PGA} - \ln m_C}{\sqrt{\beta_C^2 + \beta_{D|PGA}^2 + \beta_M^2}} \right) \quad (1)$$

where  $P(LS|PGA)$ —the probability of a structure reaching or exceeding a limit state under the action of an earthquake with a ground motion of  $PGA$  is also called the limit state probability;  $LS$ —the defined limit state;  $PGA$ —peak ground acceleration;  $\Phi(\cdot)$ —normal distribution function;  $\lambda_C$ —equal to  $\ln m_C$ , the logarithmic mean of seismic capacity  $C$ ;  $\lambda_{D|PGA}$ —equal to  $\ln m_{D|PGA}$ , when the ground motion is  $PGA$ , the logarithmic mean value of the earthquake demand  $D$ ;  $\beta_C$ —logarithmic standard deviation of seismic capacity;  $\beta_{D|PGA}$ —logarithmic standard deviation of seismic demand;  $\beta_M$ —model uncertainties, according to the literature (Ellingwood et al., 2007) take 0.2.

The seismic fragility function assumes that the seismic demand  $D$  and the seismic capacity  $C$  obey the lognormal distribution. The seismic demand parameters  $m_{D|PGA}$  and  $\beta_{D|PGA}$  are generally obtained by nonlinear time-history analysis by fitting the ground motion parameters and damage index. To obtain the probabilistic seismic demand parameters, it is necessary to carry out a large number of finite element simulations of the structure, so that the structure can obtain the seismic response of the structure under each ground motion intensity, and the selected ground motion intensity distribution should be wide and the number should be large to obtain the response data of the structure under different earthquake intensities. Based on this, the formula of the probabilistic seismic demand fitting method is:

$$\ln m_{D|PGA} = \beta_0 + \beta_1 \ln PGA \quad (2)$$

$$\beta_{D|PGA} = \sqrt{\frac{\sum_{i=1}^{N_{RTR}} [\ln D_i - \ln (m_{D|PGA})]^2}{N_{RTR} - 2}} \quad (3)$$

where  $\beta_0, \beta_1$ —linear fitting parameters;  $N_{RTR}$ —number of selected ground motion waves;  $D_i$ —the response of the finite element model is input under the action of the  $i$ th ground motion.

To obtain seismic capacity parameters  $m_C$  and  $\beta_C$ , two methods can be selected: one is to perform a nonlinear finite element random simulation of the structure to obtain the required seismic capacity parameters; the other can check the specification, according to the empirical limit given in the specification as the seismic capacity demand parameter  $m_C$ , and based on the empirical assumption of the logarithmic standard deviation of the ability. This paper mainly uses the limit value in the specification as the seismic capacity value parameter.

According to the above parameters in the seismic fragility formula (1), the limit state probability  $P(LS|PGA)$  can be calculated. The limit probability of the structure under different damage states can be calculated by the fragility function.

Then the damage state probability  $P(DS_j|PGA)$  of the structure can be obtained, and the calculation formula is:

$$P(DS_j|PGA) = \begin{cases} 1 - P(LS_1|PGA), & j = 0 \\ P(LS_{j-1}|PGA) - P(LS_j|PGA), & j = 1, 2, \dots, N-1 \\ P(LS_N|PGA), & j = N \end{cases} \quad (4)$$

where  $DS_j$ — $j$ th damage state;  $N$ —number of limit states.

According to the relationship between the limit state and the damage state, the structure is divided into  $N$  limit states by  $N+1$  damage states.

### 3 Structural Seismic Resilience Evaluation System

The seismic resilience of the structure refers to the ability of the structural system to maintain or quickly restore its use function after being affected by earthquakes, which is the ability to reflect sustainable development. At present, the methods for evaluating seismic resilience are not uniform. Some of them combine geographical, economic, and other indicators (Cimellaro et al., 2016), and some combine repair time (Dong & Frangopol, 2016). This paper mainly quotes the quantitative evaluation of structural seismic resilience based on the repair time proposed.

The seismic resilience coefficient  $R$  can be expressed as:

$$R = \int_{t_0}^{t_0+T_{LC}} \frac{Q(t)}{T_{LC}} dt \tag{5}$$

where  $t_0$ —the moment of the earthquake;  $T_{LC}$ —the control time set to evaluate the recoverability of structural functions;  $Q(t)$ —the functional function of the structural system.

$Q(t)$  is a dimensionless function of time, which is composed of the loss function and the recovery function of the system transient performance. Its expression is as follows:

$$Q(t) = 1 - [L(I, T_{RE}) \times \{H(t - t_{0E}) - H(t - (t_{0E} + T_{RE}))\}] \times f_{rec}(t, t_{0E}, T_{RE}) \tag{6}$$

where  $L(I, T_{RE})$ —loss function;  $f_{rec}$ —recovery function;  $I$ —earthquake intensity;  $T_{RE}$ —earthquake damage recovery time;  $H()$ —unit step function.

The resilience coefficient  $R$  is the integral of  $t_{0E}$  and  $t_0 + T_{LC}$  to the functional function  $Q(t)$ . The calculation of the loss function requires seismic fragility information. It can be seen from formula (6) that  $Q(t) = 1.0$  without loss and  $0 < Q(t) < 1.0$  with loss. So the recoverability can be reflected by the functional function. If there is no loss after earthquakes, then  $R = 100\%$ , otherwise the range of the resilience coefficient of structure is  $0 < R < 100\%$  when the structure loses.

Figure 1 shows the function of the system before and after earthquakes and the recovery process after earthquakes.

After the bridge structure is damaged by the earthquake, the repair time of the component determines the repair time of the whole bridge structure, so the repair time of the component directly determines the seismic resilience of the structure. In the process of component repair, the different repair methods directly affect the length of repair time.

The analysis of the seismic fragility results of the bridge can point out the exceeding probability of different damage states of the component or the whole bridge under the action of ground motion. On this basis, the corresponding post-earthquake repair time can be obtained by statistical analysis. The commonly used functional expressions are as formula (7) shows. Then the functional relationship between the post-earthquake repair time and the  $PGA$  under the action of ground motion can be ulteriorly constructed, which is the resilience function.

$$T_{RE} = \sum_{i=0}^n t_i P_i \quad (n = 1, 2, 3, 4) \tag{7}$$

where  $T_{RE}$ —recovery time of structure or component;  $i$ —damage state of structure or component;  $t_i$ —the repair time of the structure or component corresponding to the first damage state;  $P_i$ —the probability of occurrence of the  $i$ th damage state.

The occurrence probability of the  $i$ th damage state can be obtained by the exceedance probability in the fragility curve. The formula is as follows:

$$P_0 = 1 - P_{f1}; \quad P_1 = P_{f1} - P_{f2}; \quad P_2 = P_{f2} - P_{f3}; \tag{8}$$

$$P_3 = P_{f3} - P_{f4}; \quad P_4 = P_{f4}$$

After determining the repair method to further determine the repair time, based on the damage exceeding probability, it is easy to determine the recovery efficiency, that is, the resilience coefficient, which can quantitatively describe the strength of the recovery ability of the component after earthquakes. The specific calculation formula is as follows:

$$R_g = 1 - T_{RE}/T_0 \tag{9}$$

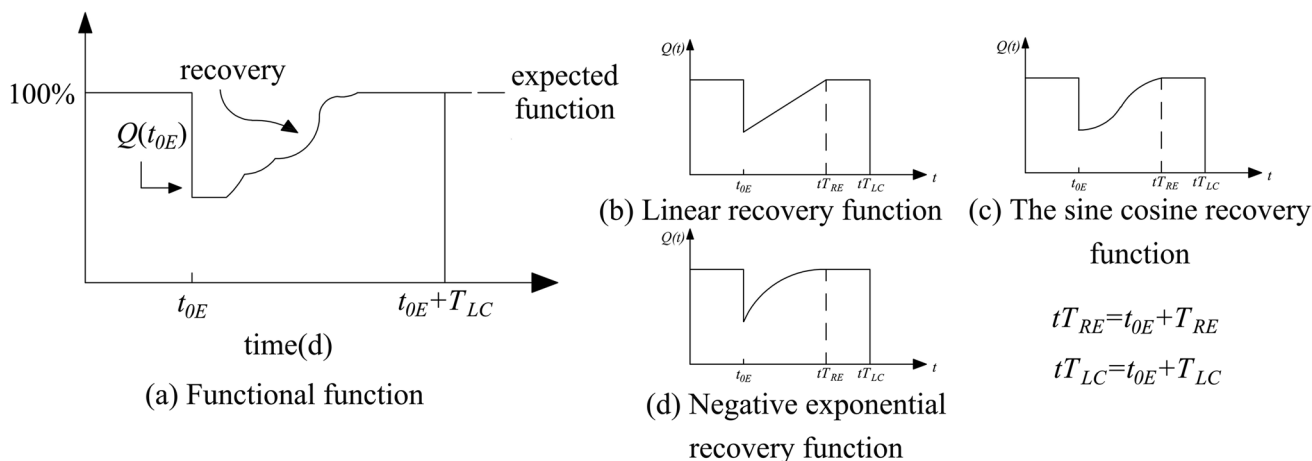


Fig. 1 Resilience index diagram and post-earthquake recovery function

where  $T_0$ —the time required for the initial construction of the component.

#### 4 Description of the Hybrid Pier

The author divides the performance objectives of the bridge structure. According to the four-level seismic fortification objectives, a new type of hybrid piers is designed based on the seismic resilience design method, which mainly relies on replaceable components to achieve repairable structural performance after earthquakes. Since the bridge is a top-heavy structure, it is easy to form a plastic zone at the lower and upper ends of the pier in the form of a single pier when encountering earthquakes. Therefore, the earthquake resilient structure is set at the bottom of the pier, which mainly includes the inner core variable cross-section round platform structure and the outer tubular structure. The outer reinforced concrete is designed as a tubular shape. To ensure that the internal structure can still be in an elastic state when the external replaceable structure of the pier is destroyed under the action of earthquakes, the shape of the inner core reinforced concrete is designed as a variable cross-section round platform with easement curves. The hybrid pier and steel bar arrangement and simplified mechanical model are shown in Fig. 2.

For the hybrid pier proposed in this paper, it can be assumed that the four displacement angles correspond to the four-level state of the pier, as shown in Table 1. The pier adopts C40 concrete, elastic modulus  $E_c = 3.25 \times 10^4$  N/mm<sup>2</sup>; HRB400 steel bar, elastic modulus  $E_s = 2.0 \times 10^5$  N/mm<sup>2</sup>. The pier height  $L = 10,000$  mm, and the pier plastic zone height  $L_p = 700$  mm, the pier diameter  $d_1 = 1000$  mm. The thickness of the replaceable structure outside the pier is  $t = 150$  mm, and the diameter of the minimum section of the inner core variable cross-section round platform structure is  $d_2 = 700$  mm.

According to the research of Sun and Tan (2022), this paper presents the phenomenon of follow-up stiffness in detail. The phenomenon of follow-up stiffness refers to the phenomenon that the damage degree of the pier increases and the stiffness of the structure decreases with the increase of the earthquake strengths under the four-level states with different earthquake strengths.

Under the influence of the follow-up stiffness phenomenon, the earthquake response spectrum of the structure under the four-level ground motions may be shown in Fig. 3a. When the earthquake is a frequent earthquake, the structure does not have any damage and is in a completely elastic state, the natural vibration period of the structure is  $T_1$ , the corresponding structural seismic influence coefficient is  $\alpha_1$ , and the horizontal seismic force acting on the structure is  $\alpha_1 G$ ; when the earthquake is a design earthquake,

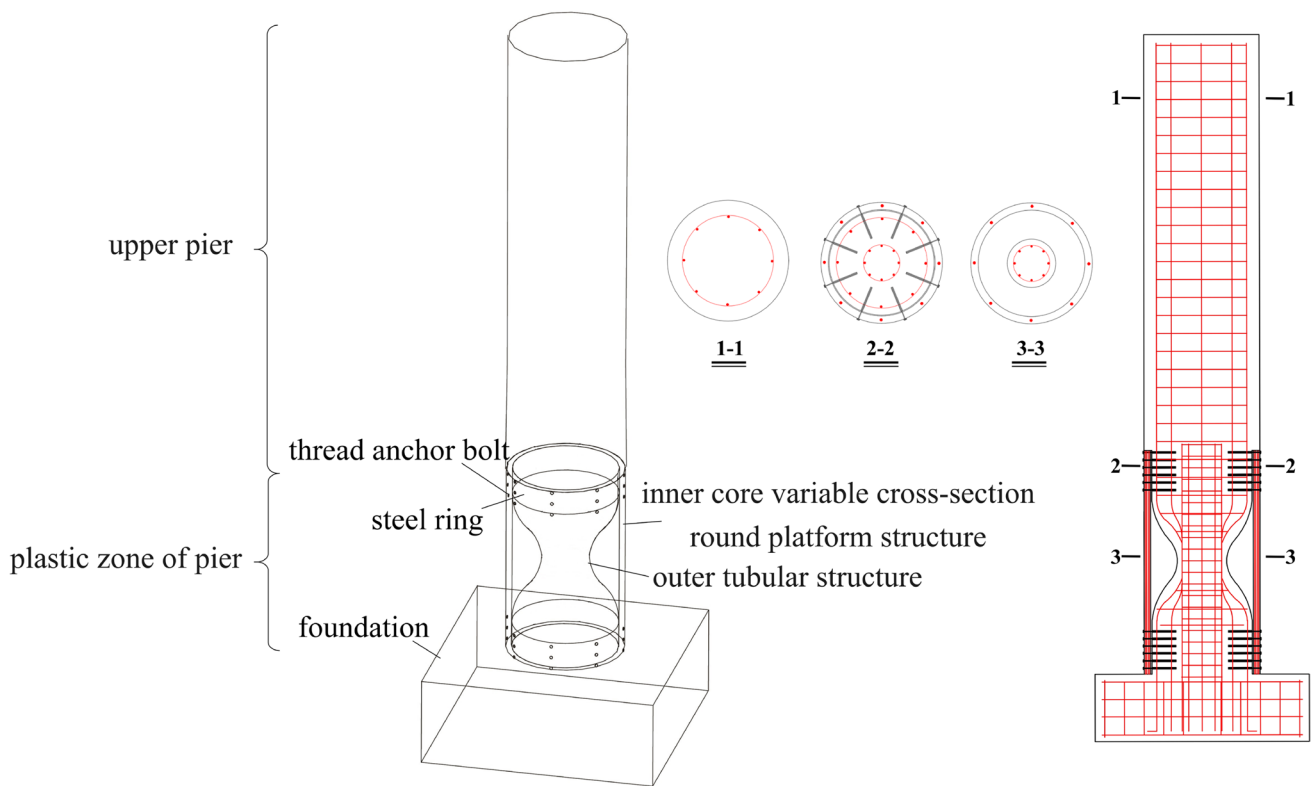
the structure begins to damage, the stiffness of the structure decreases, the natural vibration period of the structure is  $T_2$ , the corresponding structural seismic influence coefficient is  $\alpha_2$ , and the horizontal force acting on the structure is  $\alpha_2 G$ ; when the earthquake is a rare earthquake, the structure is further damaged, the stiffness of the structure is further reduced, the natural vibration period of the structure is  $T_3$ , the corresponding structural seismic influence coefficient is  $\alpha_3$ , and the horizontal force acting on the structure is  $\alpha_3 G$ ; when the earthquake is an extremely rare earthquake, the structure does not collapse, the stiffness of the structure is the smallest, the natural vibration period of the structure is  $T_4$ , the corresponding structural seismic influence coefficient is  $\alpha_4$ , and the horizontal force acting on the structure is  $\alpha_4 G$ .

Under the influence of the follow-up stiffness phenomenon, the earthquake response spectrum of the structure under extremely rare seismic waves may be shown in Fig. 3b. The four damage states of 1, 2, 3, 4 correspond to the normal use, mild damage, moderate damage, and severe damage of the structure under extremely rare seismic waves. When the structure is in the damage limit state of normal use, the natural vibration period of the structure is  $T_1$ , the corresponding structural seismic influence coefficient is  $\alpha_1$ , and the horizontal seismic force acting on the structure is  $\alpha_1 G$ ; when the structure is in the mild damage limit state, the natural vibration period of the structure is  $T_2$ , the corresponding structural seismic influence coefficient is  $\alpha_2$ , and the horizontal seismic force acting on the structure is  $\alpha_2 G$ ; when the structure is in the moderate damage limit state, the natural vibration period of the structure is  $T_3$ , the corresponding structural seismic influence coefficient is  $\alpha_3$ , and the horizontal seismic force acting on the structure is  $\alpha_3 G$ ; when the structure is in the severe damage limit state, the natural vibration period of the structure is  $T_4$ , the corresponding structural seismic influence coefficient is  $\alpha_4$ , and the horizontal seismic force acting on the structure is  $\alpha_4 G$ .

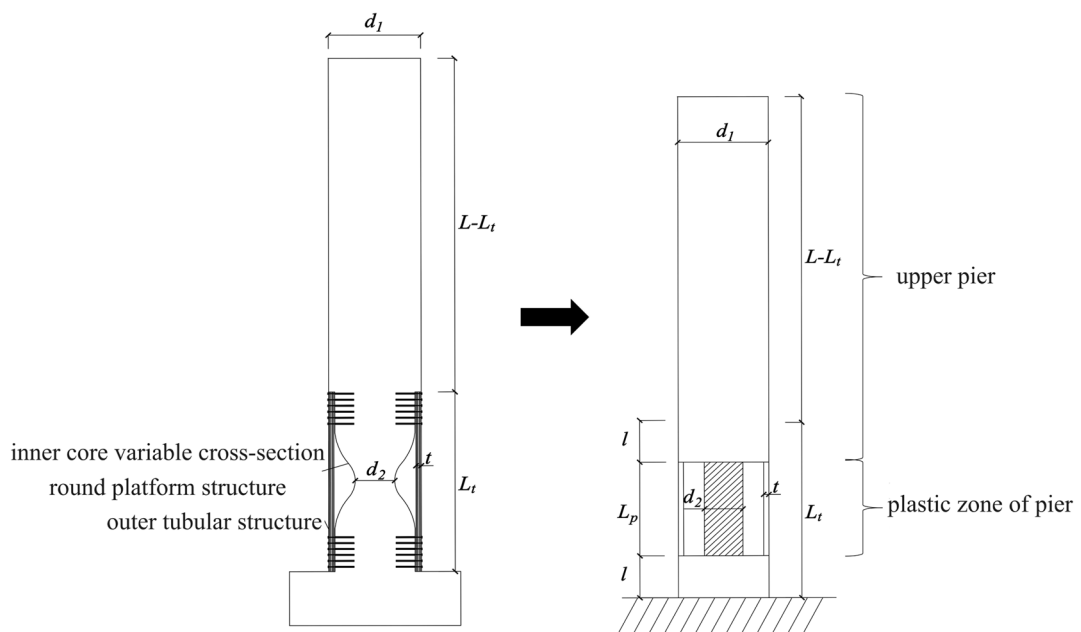
From Fig. 3a, it can be seen that the seismic influence coefficient of the structure in the four cases does not increase with the increase of the earthquake strength of the structure, but is affected by the change of the structural stiffness. If the structure design is reasonable, it can lead to decrease in the force acting on the structure with increase in the earthquake strength, which is conducive to the adaptation of the structure and the resistance to the earthquake. Such a structure has better seismic resilience. It can be seen from Fig. 3b that with the progress of the earthquake, the structure is destroyed step by step, and the stiffness of the structure is gradually degraded, which leads to the increase of the natural vibration period of the structure, and finally leads to the decrease of the seismic force acting on the structure, so that the structure has certain seismic resilience.

The inner core variable cross-section round platform structure of the earthquake resilience structure of the





(a) Hybrid pier and reinforcement layout

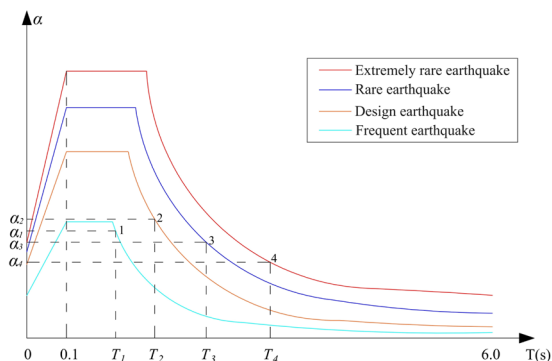


(b) Simplified mechanical model

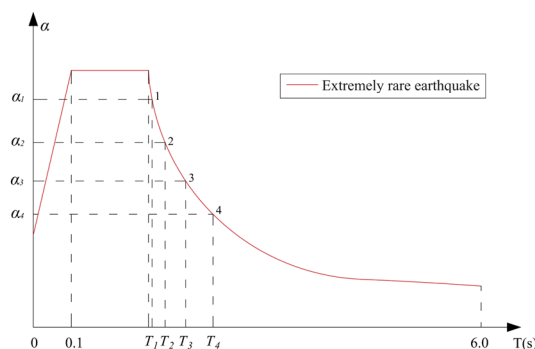
Fig. 2 Hybrid pier model and parameters

**Table 1** Four-level states of hybrid pier and repair suggestions

Damage state	Performance level	The allowable displacement angle (%)	repair suggestion
Normal use	The concrete on the tensile side of the bridge pier is cracked, and the bridge pier is in the elastic stage	0.5	There is no need to repair or repair the cracks by resin perfusion
Mild damage	The concrete of the outer tubular structure on the compression side of the pier is crushed, and the steel bar is buckled	1	Reinforcement with steel bars and smear coverage for repair
Moderate damage	Reinforcement yield of the outer tubular structure on the tensile side of the pier	2	Replacement of the outer tubular structure
Severe damage	The bearing capacity of the pier inner core variable cross-section round platform structure decreases to 85% of the maximum value	4	The inner core variable cross-section round platform structure is strengthened by carbon fiber reinforced plastic (CFRP) material or steel ring, and the outer tubular structure is replaced



(a) Four-level ground motion response spectrum under the follow-up stiffness phenomenon



(b) Extremely rare seismic waves response spectrum under the follow-up stiffness phenomenon

**Fig. 3** Different response spectra under the influence of stiffness follow-up phenomenon

hybrid pier is an integral structure with the upper pier and foundation. The function of the earthquake resilience structure is realized by repairing or replacing the outer tubular structure after earthquakes. Therefore, the internal structure and the external replaceable structure are mainly connected by the threaded anchor. To prevent the reduction of the strength caused by the weakening of the cross-section at the connection caused by the setting of the threaded anchor, a layer of steel ring is wrapped on the part of the internal structure connected with the external replaceable structure, to achieve the design goal of strong joint and weak component. Figure 4a is the joint structure diagram of the earthquake resilient structure of the hybrid pier. Figure 4b is the replacement diagram of the external replaceable structure.

## 5 Selection of Ground Motions and Determination of the Pier Damage Index

### 5.1 Selection of Ground Motions

Because the records of measured seismic waves in China are few and not comprehensive enough, the seismic waves selected in this paper are selected from the strong ground motion databases of the Pacific Earthquake Engineering Research Center (PEER) of the United States according to the type of bridge site. The near-fault ground motion wave record is different from the general ground motion wave record, and Chinese scholars often use the 20 km fault distance as the boundary to divide the near and far fault ground motion. According to the site conditions of

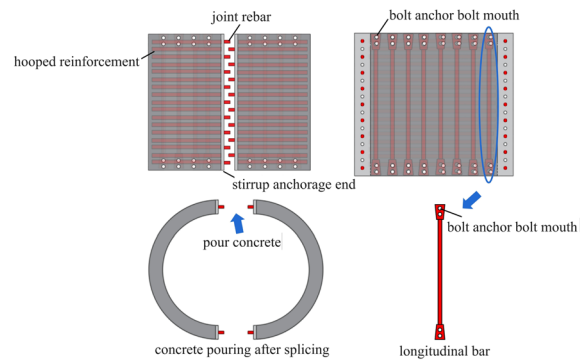
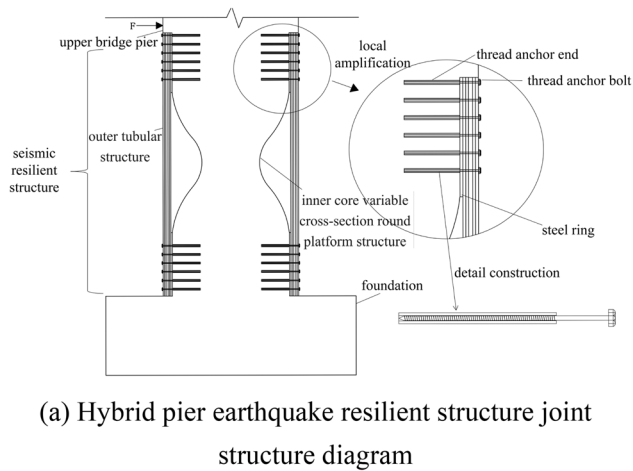
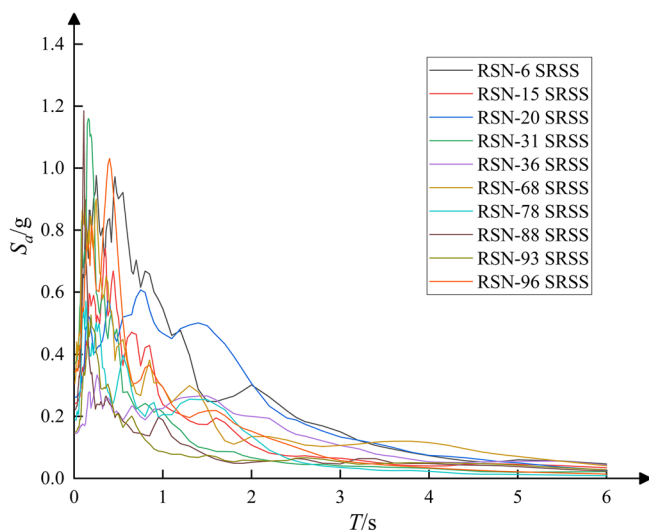


Fig. 4 Functional recovery design diagram of the hybrid pier

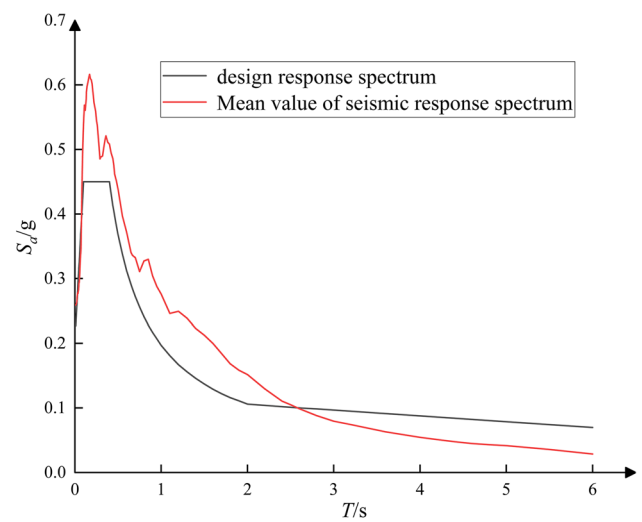
the bridge, the design response spectrum is established according to *Code for Seismic Design of Urban Bridges* (CJJ, 2011). For structural fragility analysis, it is generally believed that 10–20 seismic records can meet the accuracy requirements. Therefore, according to the difference between the Chinese code and the American code, this paper refers to the research results of Chinese scholars to obtain the site condition of type II by the Chinese code and considers the condition that the fault distance is greater than 20 km. The fitting of the mean response spectrum curve of all ground motions after amplitude modulation to

the design spectrum is shown in Fig. 5. It can be seen that the effect of the selected waves is very good, which meets the site conditions and basic wave selection requirements.

With *PGA* as the standard, the acceleration time-histories of the 10 ground motion records selected above are modulated at intervals of 0.1g in the range of 0g to 1.0g and 0.2g in the range of 1.0g to 2.0g, respectively, without changing the other parameters of the ground motion records. After amplitude modulation, 140 ground motion records are obtained, and then time-history analysis is carried out to obtain structural response data.



(a) Seismic wave response spectrum



(b) Seismic wave response spectrum mean and standard response spectrum

Fig. 5 Selection of seismic wave



## 5.2 Determination of Damage Index

In this paper, the lateral displacement angle of the pier top is used as the seismic response parameter. The limiting value of structural bearing capacity corresponding to normal use, mild damage, moderate damage, and severe damage is defined by the displacement angle of the pier top, as shown in Table 2.

## 6 Fragility Analysis of the Pier

### 6.1 Finite Element Model of the Pier

This paper selects a hybrid pier and an ordinary RC pier for a comparative analysis. The model of the hybrid pier and ordinary RC pier adopts C40 concrete, the longitudinal reinforcement and stirrup are HRB400 grade steel bar and HRB335 grade steel bar respectively. The longitudinal reinforcement ratio is 2.59%, the stirrup reinforcement ratio is 2.26%, the pier height  $L = 10,000$  mm, the pier plastic zone height  $L_p = 700$  mm, and the pier diameter  $d_1 = 1000$  mm. The thickness of the outer tubular structure of the plastic zone of the hybrid pier  $t = 150$  mm, the longitudinal reinforcement ratio is 3.77%, and the stirrup reinforcement ratio is 1.54%. The inner core variable cross-section round platform structure is equivalent to a cylindrical structure with the minimum cross-section diameter  $d_2 = 700$  mm.

In this paper, the structural analysis diagram of two piers and specific parameters of the model is shown in Fig. 6. The fragility analysis is carried out by using the finite element software OPENSEES (Salkhordeh et al., 2021; Stefanidou et al., 2024). The concrete of the protective layer of the pier section model is established by using the Concrete01 model, the Concrete02 is used to simulate the confined concrete, the steel bar is simulated by using

the Steel02 model, and the pier body is established by using the dispBeamColumn unit.

### 6.2 PSDM and Fragility Curve

The IDA curves of the hybrid pier and the ordinary RC pier are shown in Fig. 7. It can be seen from the figure that the overall trend is that the displacement angle of the pier top also increases to a certain extent with the increase of  $PGA$ . When the  $PGA$  is in a small range, the increase of the lateral displacement angle of the pier top is not large. Considering that the structure is still in the linear elastic stage at this time, it still has a good working performance. As the  $PGA$  continues to increase, the structure enters the elasto-plastic stage, and the displacement angle of the pier top also changes greatly. The response of piers to different seismic waves is quite different. When  $PGA$  is small, the displacement angle of the pier top is less affected by different seismic waves. With the increase of  $PGA$ , the influence of different seismic waves on the displacement angle of the pier top will be greatly differentiated.

Assuming that the  $PGA$  and the pier top displacement angle  $\theta$  are power exponential relationships. Linear regression was performed using the results calculated by IDA above, as shown in Fig. 8. In the linear regression function of the ordinary RC pier,  $a = 0.305$ ,  $b = 1.053$ . In the linear regression function of the hybrid pier,  $a = 0.385$ ,  $b = 0.882$ . The results are shown in formulas (10) to (11). The correlation coefficient  $R^2$  of the linear regression equation is also shown in this figure. The values of  $R^2$  are also greater than 0.7, which means that the natural logarithms of  $PGA$  and  $\theta$  satisfy the linear correlation.

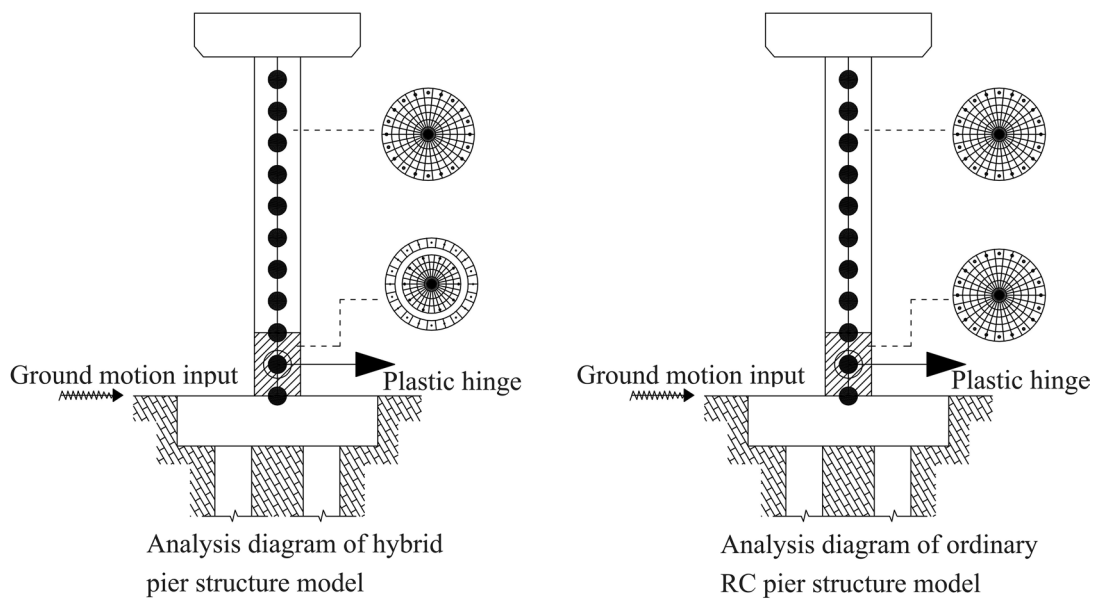
$$\ln(\theta_{RC}) = 0.305 + 1.053 \ln(PGA) \quad (10)$$

$$\ln(\theta_{HC}) = 0.385 + 0.882 \ln(PGA) \quad (11)$$

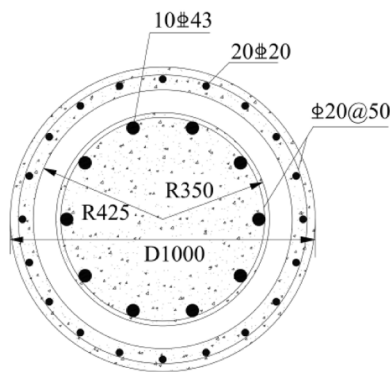
The linear regression results can be used to establish the fragility curve function equation. The seismic fragility curves of the hybrid pier and the ordinary RC pier are shown in Fig. 9a. It can be seen that with the increase of  $PGA$ , the damage probability of two different piers increases, and the fragility curves of the hybrid pier and the ordinary RC piers are close. On the whole, the exceedance damage probability of the hybrid pier is slightly larger than that of the ordinary RC pier. However, in the case of mild damage, moderate damage, and severe damage, with the increase of  $PGA$ , the exceedance damage probability of the ordinary RC pier gradually tends to be slightly larger than that of the hybrid pier, indicating that with the damage of the hybrid pier, the follow-up stiffness phenomenon gradually affects the seismic performance. The seismic force acting on the structure is

**Table 2** Bridge damage state division based on the pier top displacement angle

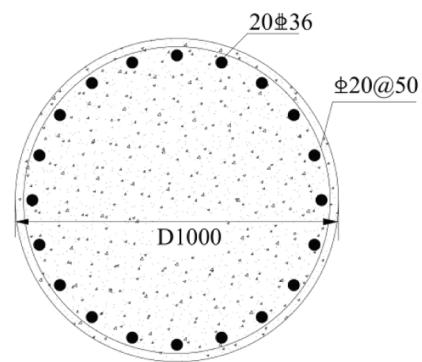
(a) Bridge damage state defined by pier top displacement angle		(b) The limiting value of structural bearing capacity under different damage states	
Damage state	Criterion	Pier top displacement angle	Limiting bearing capacity of the structure (%)
Normal use	$\theta_d < \theta_1$	$\theta_1$	0.5
Mild damage	$\theta_1 < \theta_d < \theta_2$	$\theta_2$	1
Moderate damage	$\theta_2 < \theta_d < \theta_3$	$\theta_3$	2
Severe damage	$\theta_3 < \theta_d < \theta_4$	$\theta_4$	4



(a) Structural analysis model diagram



(b) Hybrid pier plastic zone reinforcement diagram



(c) The upper pier of the hybrid pier and the ordinary RC pier reinforcement diagram

Fig. 6 Structural analysis model and specific parameters

reduced, so that its seismic performance is improved. The designed hybrid pier has better performance, but at the same time, it also shows that the designed hybrid pier needs further improvement to enhance the seismic performance in small and moderate earthquakes.

In order to further reveal the influence of the follow-up stiffness phenomenon, the IDA statistical results of the top displacement angle of the hybrid pier and the ordinary RC pier are obtained, as shown in Fig. 9b. The mean value of the displacement angle of piers under different *PGA* can reflect the average level of the displacement angle of the pier with the change of the ground motion, and the maximum value of the displacement angle of piers under different *PGA* can

reflect the maximum damage degree that piers may encounter. It can be seen from the mean displacement angle of two piers in Fig. 9b that the displacement angle of the hybrid pier and the ordinary RC pier increases with the increase of *PGA*. Due to the flexibility of the designed hybrid pier, under the action of different seismic waves, the increase of the ordinary RC pier is slightly smaller than that of the hybrid pier, but the overall difference is not large. From the maximum displacement angle of two piers, it can be seen that when the range of *PGA* is 0–0.6 g, the hybrid pier has a larger displacement angle, and when the range of *PGA* is 0.6–1.8 g, the ordinary RC pier has a larger displacement angle. The reason for this result is the follow-up stiffness

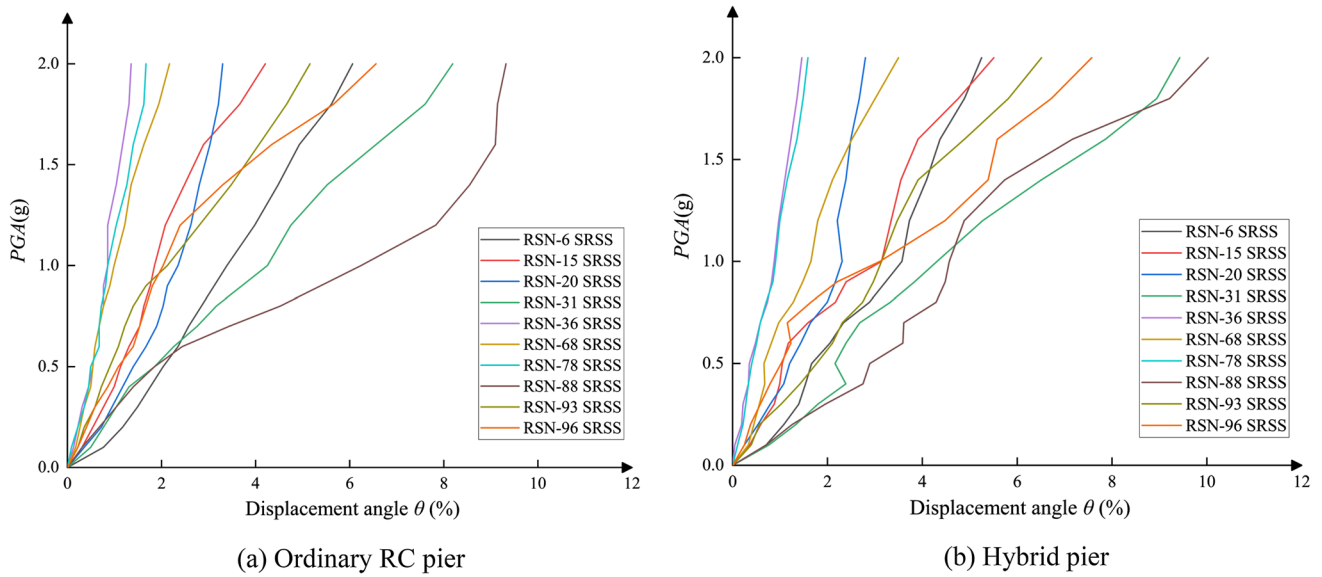


Fig. 7 IDA curves of pier top displacement angle

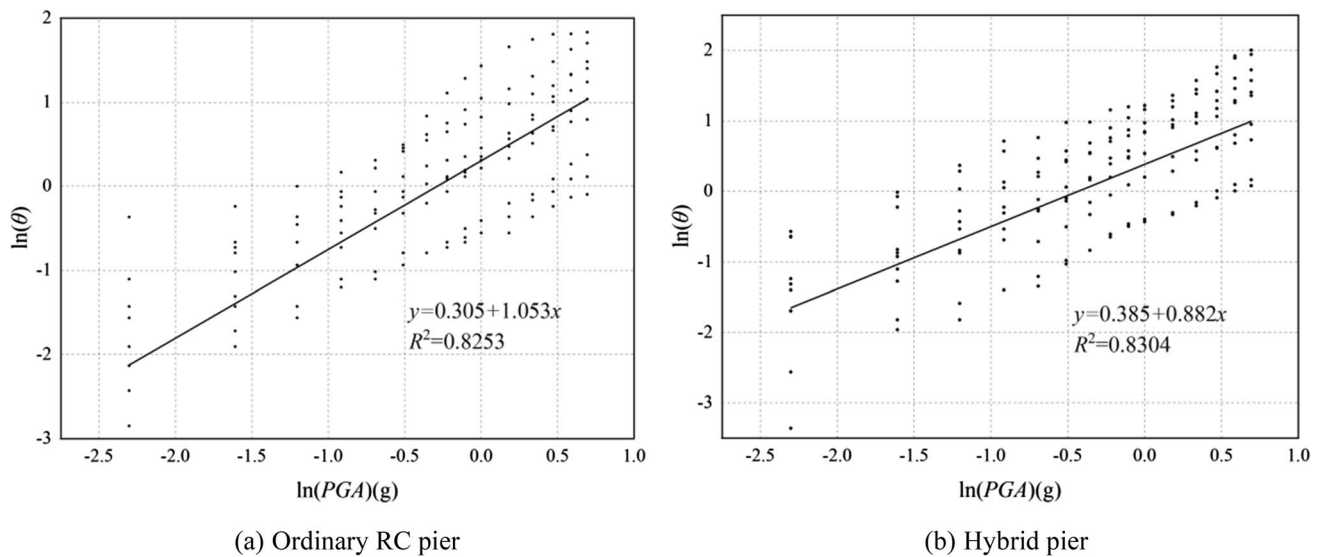


Fig. 8 Linear regression fitting curve

phenomenon, and further affects the vulnerability curves. It shows that the hybrid pier has good research significance and development prospects.

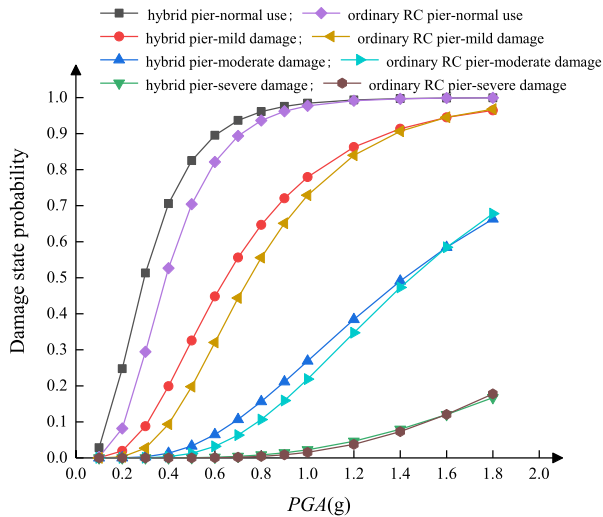
### 7 Seismic Resilience Curve of the Pier

From the obtained fragility curves, the exceeding probabilities of the hybrid pier and the ordinary RC pier at different damage states are shown in Table 3.

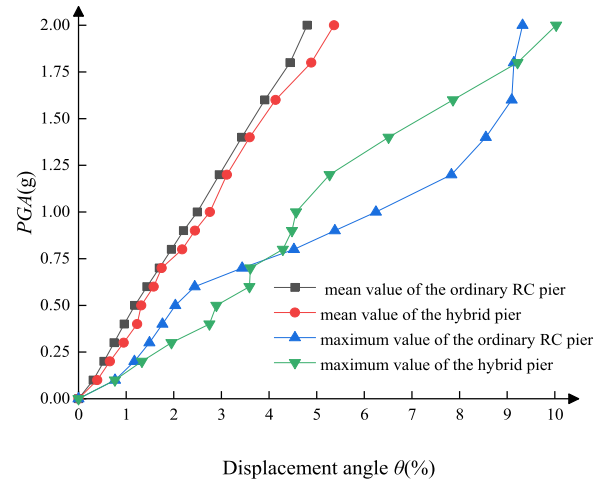
It is an important link in the seismic resilience evaluation of bridge piers to reasonably determine the

post-earthquake recovery time of bridge piers under different damage states, which affects the accuracy of the results. In this paper, the recovery time of the pier is preliminarily determined based on the existing references of the pier repair construction and the characteristics of the pier studied (Chen et al., 2022). The proposed pier recovery time is shown in Table 4.

Based on determining the repair time of each damage state of the pier, the seismic resilience coefficient of the pier can be calculated by the formula (7) to (9), as shown in Table 5, so that the corresponding seismic resilience curves can be drawn, as shown in Fig. 10.



(a) Seismic fragility curves



(b) The mean and maximum displacement angle of two piers under different *PGA*

Fig. 9 Comparison of fragility curves and IDA statistical curves of two piers

Table 3 Bridge pier damage exceeding probability

PGA(g)	0.1	0.2	0.3	0.4	0.5	0.6	0.7	0.8	0.9	1.0
Hybrid piers										
Normal use	0.0285	0.2477	0.5133	0.7057	0.8249	0.8954	0.9367	0.9611	0.9756	0.9845
Mild damage	0.0005	0.0193	0.0880	0.1989	0.3256	0.4481	0.5562	0.6469	0.7206	0.7795
Moderate damage	0.0000	0.0003	0.0031	0.0128	0.0330	0.0647	0.1066	0.1564	0.2114	0.2690
Severe damage	0.0000	0.0000	0.0000	0.0002	0.0006	0.0019	0.0043	0.0083	0.0143	0.0226
Ordinary RC piers										
Normal use	0.0022	0.0817	0.2947	0.5264	0.7041	0.8213	0.8934	0.9365	0.9620	0.9771
Mild damage	0.0000	0.0027	0.0271	0.0934	0.1977	0.3206	0.4438	0.5557	0.6510	0.7291
Moderate damage	0.0000	0.0000	0.0005	0.0034	0.0127	0.0320	0.0633	0.1063	0.1591	0.2188
Severe damage	0.0000	0.0000	0.0000	0.0000	0.0002	0.0006	0.0018	0.0042	0.0086	0.0153

Table 4 Proposed pier recovery time(d)

Damage state	Ordinary RC piers	Hybrid piers
Normal use	1	1
Mild damage	5	5
Moderate damage	28	10
Severe damage	90	45

The seismic resilience curve of the pier can intuitively describe the change in the seismic resilience of the pier with the change in earthquake intensity. From Fig. 10, it can be seen that with the increase of *PGA*, the seismic resilience coefficient of the ordinary RC pier and the hybrid pier gradually decreases. The resilience coefficient of the ordinary RC pier remains between 0.88 and 1 when *PGA* is less than 1, and the

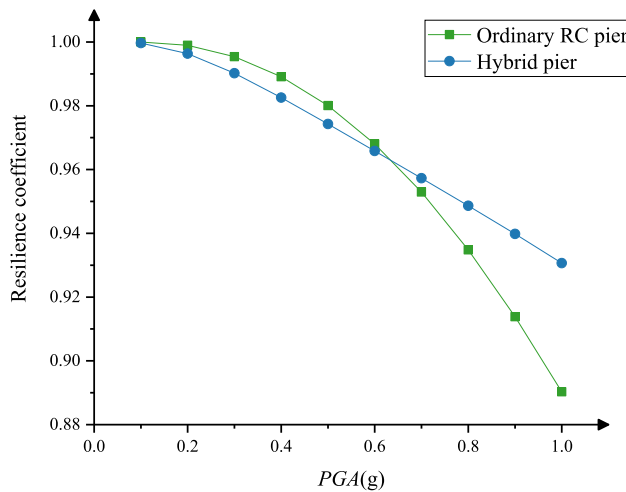
resilience performance is also good. However, the resilience coefficient of the hybrid pier is always maintained at 0.9–1, and the resilience performance is excellent. When *PGA* is small, the resilience coefficient of the hybrid pier is smaller than that of the ordinary RC pier. With the gradual increase of *PGA*, under the effect of the follow-up stiffness phenomenon, the resilience coefficient of the hybrid pier is gradually greater than that of the ordinary RC pier, so the designed hybrid pier has better seismic resilience performance.

### 8 Conclusions

In this paper, the seismic resilience of hybrid piers is studied. Firstly, the four-level seismic resilience performance objectives of the hybrid pier are proposed. On this basis, the

**Table 5** Seismic resilience coefficient of piers

PGA(g)	0.1	0.2	0.3	0.4	0.5	0.6	0.7	0.8	0.9	1.0
$T_{RE}$										
Ordinary RC pier	0.00220	0.09291	0.41360	0.97957	1.79504	2.87676	4.23541	5.86725	7.75517	9.87320
Hybrid pier	0.03045	0.32639	0.88151	1.57049	2.31451	3.07573	3.84333	4.62072	5.41650	6.23940
$R_s$										
Ordinary RC pier	0.99998	0.99897	0.99540	0.98912	0.98006	0.96804	0.95294	0.93481	0.91383	0.89030
Hybrid pier	0.99966	0.99637	0.99021	0.98255	0.97428	0.96583	0.95730	0.94866	0.93982	0.93067

**Fig. 10** Seismic resilience curves

follow-up stiffness phenomenon is found. The IDA analysis of a hybrid pier and an ordinary RC pier are carried out by OPENSEES, and the fragility curves and seismic resilience curves of two piers are compared. Summarize as follows:

1. The seismic fragility curves of the hybrid pier and the ordinary RC pier are drawn. It is found from seismic fragility curves that the damage exceeding probability of the hybrid pier is slightly greater than that of the ordinary RC pier. However, with the increase of  $PGA$ , the damage exceeding probability of the ordinary RC pier is gradually greater than that of the hybrid pier. The results indicate that after the damage of the hybrid pier, the follow-up stiffness phenomenon has an impact on the seismic performance, which reduces the seismic force acting on the structure and improves its seismic resilience.
2. The displacement angles of the hybrid pier and the ordinary RC pier obtained by IDA analysis are analyzed statistically, and the mean and maximum values of the displacement angles of two piers are obtained. Through the statistics curves of the displacement angle of the hybrid pier and the ordinary RC pier, compare the maximum value of the displacement angles of two piers, it

can be seen that when the range of  $PGA$  is 0–0.6 g, the hybrid pier has a larger displacement angle, and when the range of  $PGA$  is 0.6–1.8 g, the ordinary RC pier has a larger displacement angle. The reason for this result is the follow-up stiffness phenomenon, and further affects the vulnerability curves. It shows that the hybrid pier has good research significance and development prospects. But at the same time, it also shows that the designed hybrid pier needs further improvement to enhance the seismic performance in small or moderate earthquakes.

3. The post-earthquake recovery time of the hybrid pier and the ordinary RC pier under different damage states was determined. Combined with the fragility curves, the seismic resilience curves of two piers were reasonably drawn. It was found that the resilience coefficient of the hybrid pier was always maintained at 0.9–1, and the resilience performance was excellent. With the gradual increase of  $PGA$ , the resilience coefficient of the hybrid pier is gradually larger than that of the ordinary RC pier under the follow-up stiffness phenomenon.

**Acknowledgements** Natural Science Foundation of Shaanxi Province (Grant Nos. 2020JM-475 and 2023-JC-YB-373) and National Natural Science Foundation of China (Grant No. 51408453) are much appreciated.

**Author Contributions** Jianpeng Sun: proposed the concept of follow-up stiffness phenomenon and the preliminary structure of the hybrid pier. Weichao Xu: modified the original manuscript, table and figure. Zihan Tan: provided the original manuscript, finished the finite element analysis, the result analysis, the concrete design of the hybrid pier and the detailed description of the concept of follow-up stiffness.

## Declarations

**Conflict of interest** The authors declare that they have no known competing financial interests or personal relationships that could have influenced the work reported in this paper.

## References

- ASCE/SEI 7-10. (2010). *Minimum design loads for buildings and other structures*. American Society of Civil Engineers. <https://doi.org/10.1061/9780784412916>



- Barker, K., Ramirez-Marquez, J. E., & Rocco, C. M. (2013). Resilience-based network component importance measures. *Reliability Engineering and System Safety*, 117(9), 89–97. <https://doi.org/10.1016/j.res.2013.03.012>
- Billah, A. H. M. M., & Todorov, B. (2021). Mainshock-aftershock damage assessment of concrete bridge reinforced with shape memory alloy rebar. In *The 17th world conference on earthquake engineering*.
- Bruneau, M., Chang, S. E., Eguchi, R. T., Lee, G. C., O'Rourke, T. D., Reinhorn, A. M., Shinozuka, M., Tierney, K., Wallace, W. A., & Von Winterfeldt, D. (2003). A framework to quantitatively assess and enhance the seismic resilience of communities. *Earthquake Spectra*, 19(4), 733–752. <https://doi.org/10.1193/1.1623497>
- Chang, S. E., & Shinozuka, M. (2004). Measuring improvements in the disaster resilience of communities. *Earthquake Spectra*, 20(3), 739–755. <https://doi.org/10.1193/1.1775796>
- Chen, J., Liang, D., You, X., & Liang, H. (2022). Performance-based assessment of bridges with novel SMA-washer-based self-centering rocking piers. *Materials*, 15(19), 6589. <https://doi.org/10.3390/ma15196589>
- Cimellaro, G. P., Renschler, C., Reinhorn, A. M., & Arendt, L. (2016). PEOPLES: A framework for evaluating resilience. *Journal of Structural Engineering*, 142(10), 04016063. [https://doi.org/10.1061/\(ASCE\)ST.1943-541X.0001514](https://doi.org/10.1061/(ASCE)ST.1943-541X.0001514)
- CJJ 166-2011. (2011). *Code for seismic design of urban bridges*. China Planning Press.
- Dion, C., Bouaanani, N., Tremblay, R., Lamarche, C. P., & Leclerc, M. (2011). Real-time dynamic substructuring testing of viscous seismic protective devices for bridge structures. *Engineering Structures*, 33(12), 3351–3363. <https://doi.org/10.1016/j.engstruct.2011.06.021>
- Dong, Y., & Frangopol, D. M. (2015). Risk and resilience assessment of bridges under mainshock and aftershocks incorporating uncertainties. *Engineering Structures*, 83(2), 198–208. <https://doi.org/10.1016/j.engstruct.2014.10.050>
- Dong, Y., & Frangopol, D. M. (2016). Performance-based seismic assessment of conventional and base-isolated steel buildings including environmental impact and resilience. *Earthquake Engineering and Structural Dynamics*, 45(5), 739–756. <https://doi.org/10.1002/eqe.2682>
- El-Bahey, S., & Bruneau, M. (2011). Buckling restrained braces as structural fuses for the seismic retrofit of reinforced concrete bridge bents. *Engineering Structures*, 33(3), 1052–1061. <https://doi.org/10.1016/j.engstruct.2010.12.027>
- El-Bahey, S., & Bruneau, M. (2012). Bridge piers with structural fuses and bi-steel columns. I: Experimental testing. *Journal of Bridge Engineering*, 17(1), 25–35. [https://doi.org/10.1061/\(ASCE\)BE.1943-5592.0000234](https://doi.org/10.1061/(ASCE)BE.1943-5592.0000234)
- Ellingwood, B. R., Celik, O. C., & Kinali, K. (2007). Fragility assessment of building structural systems in mid-America. *Earthquake Engineering and Structural Dynamics*, 36(13), 1935–1952. <https://doi.org/10.1002/eqe.693>
- Elnashai, A. S., & Di Sarno, L. (2015). *Fundamentals of earthquake engineering: From source to fragility*. Wiley.
- EN 1998-1. (2005). *Eurocode 8: Design of structures for earthquake resistance-part 1: General rules, seismic actions and rules for buildings*. European Committee for Standardization.
- Frangopol, D. M., & Bocchini, P. (2011). Resilience as optimization criterion for the rehabilitation of bridges belonging to a transportation network subject to earthquake. In *Structures congress 2011*.
- GB 18306-2015. (2015). *Seismic ground motion parameters zonation map of China*. China Standardization Administration.
- Gidaris, I., Padgett, J. E., Barbosa, A. R., Chen, S., Cox, D., Webb, B., & Cerato, A. (2017). Multiple-hazard fragility and restoration models of highway bridges for regional risk and resilience assessment in the United States: State-of-the-art review. *Journal of Structural Engineering*, 143(3), 04016188. [https://doi.org/10.1061/\(ASCE\)ST.1943-541X.0001672](https://doi.org/10.1061/(ASCE)ST.1943-541X.0001672)
- Guo, T., Cao, Z., Xu, Z., & Lu, S. (2016). Cyclic load tests on self-centering concrete pier with external dissipators and enhanced durability. *Journal of Structural Engineering*, 142(1), 04015088. [https://doi.org/10.1061/\(ASCE\)ST.1943-541X.0001357](https://doi.org/10.1061/(ASCE)ST.1943-541X.0001357)
- Karamlou, A., & Bocchini, P. (2017). Functionality-fragility surfaces. *Earthquake Engineering and Structural Dynamics*, 46(10), 1687–1709. <https://doi.org/10.1002/eqe.2878>
- Kilaniotis, I., & Sextos, A. (2019a). Impact of earthquake-induced bridge damage and time evolving traffic demand on the road network resilience. *Journal of Traffic and Transportation Engineering (english Edition)*, 6(1), 35–48. <https://doi.org/10.1016/j.jtte.2018.07.002>
- Kilaniotis, I., & Sextos, A. (2019b). Integrated seismic risk and resilience assessment of roadway networks in earthquake prone areas. *Bulletin of Earthquake Engineering*, 17(2), 181–210. <https://doi.org/10.1007/s10518-018-0457-y>
- Kiremidjian, A., Moore, J., Fan, Y. Y., Yazlali, O., Basoz, N., & Williams, M. (2007). Seismic risk assessment of transportation network systems. *Journal of Earthquake Engineering*, 11(3), 371–382. <https://doi.org/10.1080/13632460701285277>
- Li, L., Luo, G., Wang, Z., Zhang, Y., & Zhuge, Y. (2021). Prediction of residual behaviour for post-earthquake damaged reinforced concrete column based on damage distribution model. *Engineering Structures*, 234(9), 111927. <https://doi.org/10.1016/j.engstruct.2021.111927>
- Manyena, S. B. (2006). The concept of resilience revisited. *Disasters*, 30(4), 434–450. <https://doi.org/10.1111/j.0361-3666.2006.00331.x>
- Otsuka, H., Kunki, S., Park, J. G., Suzuki, Y., & Tsuchida, T. (1999a). Study on the seismic isolation of high-elevated rigid frame bridge with double deck. *WIT Transactions on the Built Environment*, 41(2), 207–216. <https://doi.org/10.2495/ERES990211>
- Otsuka, H., Yabuki, W., Nei, H., Tsutsumi, T., Maritomi, M., & Okada, T. (1999b). The investigation of earthquake resistance for the PC continuous rigid frame bridge considering nonlinearity in superstructure. *WIT Transactions on the Built Environment*, 41(2), 197–206. <https://doi.org/10.2495/ERES990201>
- Ou, Y., Chiewanichakorn, M., Ahn, I., Aref, A. J., Chen, S. S., Filiatrault, A., & Lee, G. C. (2006). Cyclic performance of precast concrete segmental bridge columns: Simplified analytical and finite element studies. *Transportation Research Record*, 1976(1), 66–74. <https://doi.org/10.1177/0361198106197600108>
- Ouyang, M., Dueñas-Osorio, L., & Min, X. (2012). A three-stage resilience analysis framework for urban infrastructure systems. *Structural Safety*, 36(5), 23–31. <https://doi.org/10.1016/j.strusafe.2011.12.004>
- Paredes, R., & Dueñas-Osorio, L. (2015). A time-dependent seismic resilience analysis approach for networked lifelines. In *International conference on applications of statistics and probability*. <https://doi.org/10.14288/1.0076219>
- Reed, D. A., Kapur, K. C., & Christie, R. D. (2009). Methodology for assessing the resilience of networked infrastructure. *IEEE Systems Journal*, 3(2), 174–180. <https://doi.org/10.1109/JSYST.2009.2017396>
- Rouse, J. M. (2004). *Behavior of bridge piers with ductile fiber reinforced hinge regions and vertical, unbonded post-tensioning*. Cornell University.
- Salkhordeh, M., Govahi, E., & Mirtaheri, M. (2021). Seismic fragility evaluation of various mitigation strategies proposed for bridge piers. *Structures*, 33(5), 1892–1905. <https://doi.org/10.1016/j.istruc.2021.05.041>
- Stefanidou, D. S., Markogiannaki, D. O., Mikes, I., & Fragiadakis, M. (2024). Fragility analysis framework for bridges subjected to



- successive natural hazards. *Structural Engineering International*. <https://doi.org/10.1080/10168664.2023.2273464>
- Sun, J., & Tan, Z. (2022). Seismic resilience-based design method for hybrid bridge pier under four-level seismic fortifications. *International Journal of Steel Structures*, 22(5), 1578–1593. <https://doi.org/10.1007/s13296-022-00666-3>
- Sun, J., Tan, Z., Zhang, J., Sun, W., & Zhu, L. (2023). Parameter sensitivity study on static and dynamic mechanical properties of the spatial Y-shaped tied arch bridge. *International Journal of Steel Structures*, 23(2), 458–479. <https://doi.org/10.1007/s13296-022-00705-z>
- Wang, C., Qu, Z., Shen, Y., Jiang, J., Yin, C., & Zong, Y. (2022a). Numerical investigation of the performance of segmental CFST piers with external energy dissipators under lateral cyclic loadings. *Materials*, 15(19), 6993. <https://doi.org/10.3390/ma15196993>
- Wang, C., Qu, Z., Shen, Y., Ping, B., & Xie, J. (2022b). Cyclic testing on seismic behavior of segmental assembled CFST bridge pier with external replaceable energy dissipator. *Metals*, 12(7), 1156. <https://doi.org/10.3390/met12071156>
- Wang, Z., Wang, J. Q., Tang, Y. C., Liu, T. X., Gao, Y. F., & Zhang, J. (2018). Seismic behavior of precast segmental UHPC bridge columns with replaceable external cover plates and internal dissipaters. *Engineering Structures*, 177(24), 540–555. <https://doi.org/10.1016/j.engstruct.2018.10.012>
- Xia, X., Zhang, X., & Wang, J. (2021). Shaking table test of a novel railway bridge pier with replaceable components. *Engineering Structures*, 232(7), 111808. <https://doi.org/10.1016/j.engstruct.2020.111808>
- Zhu, S., & Wang, B. (2021). Towards earthquake resilience: using superelastic SMA for high-performance seismic-resistant structures. In *17th world conference on earthquake engineering*.

**Publisher's Note** Springer Nature remains neutral with regard to jurisdictional claims in published maps and institutional affiliations.

Springer Nature or its licensor (e.g. a society or other partner) holds exclusive rights to this article under a publishing agreement with the author(s) or other rightsholder(s); author self-archiving of the accepted manuscript version of this article is solely governed by the terms of such publishing agreement and applicable law.